Stability analysis for an optical bistable dye system

Shang-qing Gong
Institute of Physics, Academia Sinica, P.O. Box 603, Beijing 100080, China
and Shan-dong Normal University, Jinan 250014, China

Shao-hua Pan and Guo-zhen Yang
China Center of Advanced Science and Technology (World Laboratory), P.O. Box 8730, Beijing 100080, China
*and Institute of Physics, Academia Sinica, P.O. Box 603, Beijing 100080, China**

(Received 27 May 1992)

A different set of the Maxwell-Bloch equations describing optical bistability in a dye ring cavity has been derived. A complete linear stability analysis including propagation effects is given. The corresponding numerical simulations show that the bistable regions are functions of both the frequency detuning and the band-structure parameters such as the bandwidth and the distribution of the dipole moments.

PACS number(s): 42.65.Pc, 42.55.Mv

I. INTRODUCTION

Recently, Fu and Haken proposed a band model of the dye molecules [1]. By using this model and linear stability analysis for the Maxwell-Bloch equations, they showed that the dye laser has a low threshold instability, which is in good agreement with the experiments done by Hillman *et al.* [2]. The relevant energy-level diagram of the band model is illustrated in Fig. 1; it consists of an excited singlet state and a continuous bandlike ground state with many vibronic sublevels. The relevance of these sublevels is evidenced by the very wide spectral tunability (several hundred angstroms) of dye lasers.

In our previous paper [3], denoted as paper I, we investigated theoretically the optical bistability in a unidirectional cavity in terms of the band model, describing the steady-state behavior and bistable regime of the coupled system (molecules plus radiation field) by the derived Maxwell-Bloch equations. We found that optical bistability can be realized over a wide frequency range.

On the basis of paper I we derive in this paper, taking into account propagation effects, a different set of Maxwell-Bloch equations which are very suitable for describing the dynamical behavior of the optical bistable system. By using this set of equations and linear stability analysis, we determine the bistable region for this system. The corresponding numerical calculations show that the bistable region depends on not only the frequency detuning but also the band structure. The stability analysis including the propagation effects also shows that there is no self-pulsing instability in the bistable system with typical dye molecules. These results are helpful to experimental studies on such bistable systems.

The paper is organized as follows: the Maxwell-Bloch equations are shown in Sec. II, a linear stability analysis is given in Sec. III and the numerical analysis is presented in Sec. IV. Section V gives a brief summary of the results in this paper.

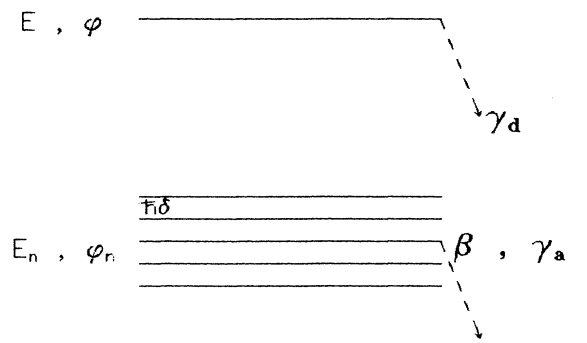

FIG. 1. Relevant energy diagram for an ideal dye molecule. E and φ (E_n and φ_n) represent the singlet excited state (sublevels of the ground state), $\hbar\delta$ is the sublevel spacing, and γ_d, β, and γ_a denote the decay rates.

II. MAXWELL-BLOCH EQUATIONS

In paper I, we obtained the following Maxwell-Bloch equations describing the interaction between the light and molecules in a dye ring cavity:

$$\dot{u}_n = -\beta u_n + (\Delta_n - \Delta) v_n \ , \tag{1}$$

$$\dot{v}_n = -\beta v_n - (\Delta_n - \Delta) u_n + \frac{f_n \theta^2 A}{\hbar} (w - w_n) \ , \tag{2}$$

$$\dot{w}_n = -\gamma_a w_n + \frac{A}{2\hbar} v_n \ , \tag{3}$$

$$\dot{w} = -\gamma_d (1 + w) - \frac{A}{2\hbar} \sum_n v_n \ , \tag{4}$$

$$\dot{A} = -c \frac{\partial A}{\partial z} + 2\pi N \omega \sum_n v_n \ , \tag{5}$$

where the meanings of these variables and parameters have been explained in paper I.

The coherent field A_I enters the cavity from the left and drives the dye molecules, as shown in Fig. 2. For simplicity, we assume that mirrors 3 and 4 have 100%

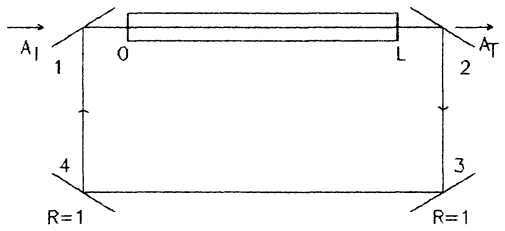

FIG. 2. Ring cavity with injection. A_I and A_T are the amplitudes of the incident and transmitted beams, respectively.

reflectivity, and we call R and T $(R+T=1)$ the reflection and transmission coefficients of mirrors 1 and 2. Taking into account the propagation effects, the boundary conditions for Eq. (5) in the ring cavity are [4]

$$A(0,t)=\sqrt{T}\,A_I+R\,A\left[L,t-\frac{\mathcal{L}-L}{c}\right], \tag{6}$$

$$A(L,t)=\frac{1}{\sqrt{T}}\,A_T(t), \tag{7}$$

where L is the length of the molecular sample and $\mathcal{L}=2(L+l)$.

We consider the commonly used limit [5]

$$\alpha L\ll 1,\quad T\ll 1,\quad \frac{\alpha L}{2T}=\text{const}, \tag{8}$$

where α is the typical linear absorption coefficient per unit length [3]. In this limiting case we can obtain the maximum physical insight and the maximal amount of analytical results. Using the stationary solution of Eqs. (1)–(5) in the limit (8), the Maxwell equation (5) and boundary condition (6) can be reformulated as

$$\frac{\partial A}{\partial t'}+c\frac{L}{\mathcal{L}}\frac{\partial A}{\partial z}=-\kappa\left[A-\frac{A_I}{\sqrt{T}}\right]+2\pi N\omega\frac{L}{\mathcal{L}}\sum_n v_n, \tag{9}$$

and

$$A(0,t')=A(L,t'). \tag{10}$$

In these equations, the time variable t' is defined by

$$t'=t+\frac{\mathcal{L}-L}{c}\frac{z}{L}, \tag{11}$$

and the cavity linewidth κ is given by

$$\kappa=\frac{cT}{\mathcal{L}}. \tag{12}$$

Equation (9) shows the reduction by a factor of $L/\mathcal{L}$ for the propagation velocity and the coupling constant. This factor arises from the geometry of the cavity [5].

It is suitable to express the time-evolution equations in terms of the normalized quantities

$$u_n=u_n'\left[\frac{r_d}{\beta}\right]^{1/2}\theta,\quad v_n=v_n'\left[\frac{r_d}{\beta}\right]^{1/2}\theta,\quad w=w',$$
$$w_n=w_n',\quad A=A'\frac{\hbar(r_d\beta)^{1/2}}{\theta}, \tag{13}$$

then Eqs. (9) and (1)–(4) become

$$\dot{u}_n'=-\beta u_n'+(\Delta_n-\Delta)v_n', \tag{14}$$

$$\dot{v}_n'=-\beta v_n'-(\Delta_n-\Delta)u_n'+\beta f_n A'(w'-w_n'), \tag{15}$$

$$\dot{w}_n'=-\gamma_a w_n'+\tfrac{1}{2}\gamma_d A' v_n', \tag{16}$$

$$\dot{w}'=-\gamma_d(1+w')-\tfrac{1}{2}\gamma_d A'\sum_n v_n', \tag{17}$$

$$\dot{A}'+c\frac{L}{\mathcal{L}}\frac{\partial A'}{\partial z}=-\kappa\left[A'-\frac{A_I}{\sqrt{T}}-2C\sum_n v_n'\right]. \tag{18}$$

The difference between the new equations (14)–(18) and the original equations (1)–(5) arises from the fact that most of the information contained in the boundary condition (6) has been transferred into the time-evolution equation for the field equation (18). Equations (14)–(18) provide a more suitable tool to study the dynamical behavior of the bistable system.

It is straightforward to calculate the stationary solution from Eqs. (14)–(18). In fact, in the limit (8), the steady-state fields are uniform in space, so that one must set not only $\dot{A}'=\dot{u}_n'=\dot{v}_n'=\dot{w}_n'=\dot{w}'=0$, but also $\partial A'/\partial z=0$. In such a way, we obtain

$$y=x+\frac{2Cxg(\Delta')}{1+\frac{1}{2}x^2 g(\Delta')}, \tag{19}$$

where $x=A^{(0)}$, $y=A_I/\sqrt{T}$, $C=\alpha L/2T$, and g is the resonant factor defined by [3]

$$g(\Delta')=\sum_n\frac{f_n}{1+(\Delta_n'-\Delta')^2+\frac{1}{2}\gamma f_n x^2}, \tag{20}$$

where we have introduced the notation

$$\Delta'=\frac{\Delta}{\beta},\quad \Delta_n'=\frac{\Delta_n}{\beta},\quad \gamma=\frac{\gamma_d}{\gamma_a}. \tag{21}$$

Equation (19) is the same as Eq. (25) of paper I. Thus, from Eqs. (14)–(18), we can also obtain the equation describing the bistable behavior in this system just as in paper I.

III. LINEAR STABILITY ANALYSIS

We consider the situation for $\gamma\ll 1$ just as in paper I, where w_n' are much smaller than u_n', v_n', w', and A' in Eqs. (14)–(18) and can be ignored. By dropping all the primes of the normalized quantities u_n' etc. and by setting $\tau=\beta t'$, Eqs. (14)–(18) become

$$\dot{u}_n=-u_n+(\Delta_n'-\Delta')v_n, \tag{22}$$

$$\dot{v}_n=-v_n-(\Delta_n'-\Delta')u_n+f_n Aw, \tag{23}$$

$$\dot{w}=-\gamma_d'(1+w)-\tfrac{1}{2}\gamma_d' A\sum_n v_n, \tag{24}$$

$$\dot{A}+q\frac{\partial A}{\partial z}=-\kappa'\left[A-\frac{A_I}{\sqrt{T}}-2C\sum_n v_n\right], \tag{25}$$

where the quantities q, κ', and γ_d' are, respectively, defined by

$$q=\frac{c}{\beta}\frac{L}{\mathcal{L}},\quad \kappa'=\frac{\kappa}{\beta},\quad \gamma'_d=\frac{\gamma_d}{\beta}\ . \tag{26}$$

Letting all the derivatives in Eqs. (22)–(25) be zero, we obtain the stationary solution of Eqs. (22)–(25) to be

$$\sum_n v_n^{(0)}=-\frac{xg}{1+\frac{1}{2}x^2g},\quad w^{(0)}=-\frac{1}{1+\frac{1}{2}x^2g}\ , \tag{27}$$

and the equations for $u_n^{(0)}$ and $x=A^{(0)}$, where

$$g=\sum_n \frac{f_n}{1+(\Delta'_n-\Delta')^2}\ . \tag{28}$$

To study the stability of the steady state we consider small perturbations δu_n, δv_n, δw, and δA for the stationary solution and make the ansatz

$$(\delta u_n,\delta v_n,\delta w,\delta A)=(x_n,y_n,d,e)\exp\left[\lambda\tau-i\frac{Q}{q}z\right]\ . \tag{29}$$

Taking the deviated quantities, which are equal to the stationary solution (27) plus the ansatz (29) in Eqs. (22)–(25), we obtain in the linear regime

$$\lambda x_n=-x_n+(\Delta'_n-\Delta')y_n\ , \tag{30}$$

$$\lambda y_n=-y_n-(\Delta'_n-\Delta')x_n+f_n(A^{(0)}d+w^{(0)}e)\ , \tag{31}$$

$$\lambda d=-\gamma'_d\left[d+\tfrac{1}{2}A^{(0)}\sum_n y_n+\tfrac{1}{2}e\sum_n v_n^{(0)}\right]\ , \tag{32}$$

$$(\lambda-iQ)e=-\kappa'\left[e-2C\sum_n y_n\right]\ . \tag{33}$$

From Eqs. (30)–(33) and the stationary solution (27), after some calculations, we derive the characteristic equation

$$\frac{\lambda-iQ}{\kappa'}=-1-\frac{2C}{1+\Lambda g}\frac{(1+\lambda/\gamma'_d-g\Lambda)F(\lambda)}{1+\lambda/\gamma'_d+\Lambda F(\lambda)}\ . \tag{34}$$

Here $\Lambda=\frac{1}{2}x^2$ is the transmitted intensity and $F(\lambda)$ is the band-structure function defined by

$$F(\lambda)=\sum_n \frac{(1+\lambda)f_n}{(1+\lambda)^2+(\Delta'_n-\Delta')^2}\ , \tag{35}$$

which depends on the bandwidth, the distribution of the dipole moments f_n, and the detuning Δ' of the field carrier frequency ω from the central transition frequency ω_0.

The stability of the stationary solution (27) is determined by the value $\mathrm{Re}\lambda$, the real part of λ. The stationary solution is stable if $\mathrm{Re}\lambda<0$, and it is unstable if $\mathrm{Re}\lambda>0$. From Eqs. (34) and (35) we can see that, generally, the instability of the optical bistable system relates not only to the band structure such as f_n and the bandwidth but also to the transmitted intensity Λ. Since the instability is actually independent of the cavity linewidth κ' [1], we need only consider the limiting case $\kappa'\to 0$. From Eq. (33) we can see that $\lambda=-iQ$ as $\kappa'=0$. Letting

$$\lambda=iQ+\lambda_1\kappa'\ , \tag{36}$$

we find from Eq. (34) that

$$\lambda_1=-1-\frac{2C}{1+\Lambda g}\frac{(1+iQ/\gamma'_d-g\Lambda)F(iQ)}{1+iQ/\gamma'_d+\Lambda F(iQ)}\ . \tag{37}$$

Let us now study the stability of the steady states using Eq. (37).

First, we set the transmitted intensity $\Lambda=0$. It is easy to prove from Eq. (37) that $\mathrm{Re}\lambda_1<0$, and therefore the eigenvalue (36) has a negative real part regardless of the value of Q, namely, the steady state is stable when the transmitted intensity approaches zero. With increasing transmitted intensity Λ, the stationary solution loses its stability if λ_1 arrives at a critical point at which [1]

$$\mathrm{Re}\lambda_1=0,\quad \frac{\partial\,\mathrm{Re}\lambda_1}{\partial Q}=0\ . \tag{38}$$

Since there are only two variables Q and Λ, Eq. (38) determines the threshold uniquely. Using the auxiliary function

$$\begin{aligned}H(Q,\Lambda)\equiv&(1+\Lambda g+2C\,\mathrm{Re}F)\left[1+\frac{Q^2}{\gamma'^2_d}\right]\\&+(1+\Lambda g-2Cg)\Lambda^2|F|^2+2\Lambda(1+\Lambda g-Cg)\mathrm{Re}F\\&+2\Lambda(1+\Lambda g-Cg)\frac{Q}{\gamma'_d}\mathrm{Im}F+2C\Lambda|F|^2\ ,\end{aligned} \tag{39}$$

where $\mathrm{Re}F$, $\mathrm{Im}F$, and $|F|$ are, respectively, the real part, imaginary part, and absolute value of $F(Q)$. We can show that Eq. (38) is equivalent to

$$H(Q,\Lambda)=0,\quad \frac{\partial H}{\partial Q}=0\ , \tag{40}$$

which is a more convenient form in calculation.

We consider the resonant mode for which the cavity frequency ω_c is nearest to the incident frequency ω, or equivalently, $Q=(0)$ [5]. In this case, Eq. (37) becomes

$$\lambda_1=-1-\frac{2C(1-g\Lambda)g}{(1+\Lambda g)^2}\ . \tag{41}$$

Letting $\lambda_1>0$, we obtain the instability condition

$$\Lambda_m(\Delta')<\Lambda<\Lambda_M(\Delta')\ , \tag{42}$$

where

$$\Lambda_m(\Delta')\equiv C\left[1-\frac{1}{Cg(\Delta')}-\left[1-\frac{4}{Cg(\Delta')}\right]^{1/2}\right]\ ,$$

$$\Lambda_M(\Lambda')\equiv C\left[1-\frac{1}{Cg(\Delta')}+\left[1-\frac{4}{Cg(\Delta')}\right]^{1/2}\right]\ .$$

The above relation (42) must be combined with the following condition for the existence of steady states [3]:

$$Cg(\Delta')>4\ . \tag{43}$$

It is easy to verify that the unstable region (Λ_m,Λ_M) corresponds to the part of the curve $x(y)$ with negative slope, namely, $dy/dx<0$ within (x_m,x_M) as shown in Fig. 3, where

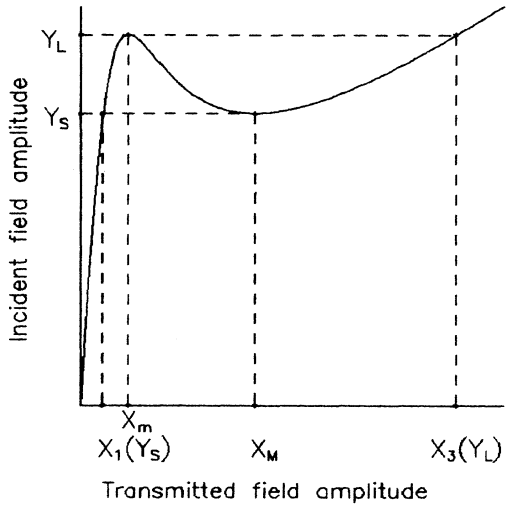

FIG. 3. Stationary-solution $x(y)$ diagram, where y and x are, respectively, proportional to the incident and transmitted fields. $(x_1(y_S),x_m)$ and $(x_M,x_3(y_L))$ are the bistable regions, whereas (x_m,x_M) is the unstable region.

$$x_m=(2\Lambda_m)^{1/2}=\sqrt{2C}\left[1-\frac{1}{Cg(\Delta')}-\left[1-\frac{4}{Cg(\Delta')}\right]^{1/2}\right]^{1/2}, \tag{44}$$

$$x_m=(2\Lambda_m)^{1/2}=\sqrt{2C}\left[1-\frac{1}{Cg(\Delta')}+\left[1-\frac{4}{Cg(\Delta')}\right]^{1/2}\right]^{1/2}. \tag{45}$$

Let y_S and y_L be the incident fields corresponding to, respectively, the transmitted fields x_M and x_m, as in Fig. 3. Note that the larger y_L corresponds to x_m, and the smaller y_S corresponds to x_M. From Eq. (19) we obtain

$$y_S=x_M+\frac{2Cx_Mg(\Delta')}{1+\frac{1}{2}x_M^2g(\Delta')}, \tag{46}$$

$$y_L=x_m+\frac{2Cx_mg(\Delta')}{1+\frac{1}{2}x_m^2g(\Delta')}. \tag{47}$$

The hysteresis cycle of transmitted versus incident fields occurs in the region (y_S,y_L). That is, there are three sets of stationary solutions $x_1<x_2<x_3$ within (y_S,y_L) in which x_2 is unstable, whereas both x_1 and x_3 are stable, corresponding to a bistable situation.

According to the relation between roots and coefficients of a cubic equation, we find from Eq. (19) the following relation:

$$x_1x_2x_3=\frac{2y}{g(\Delta')}. \tag{48}$$

Since $x_1(y_S)$, x_M, and $x_3(y_S)$ all correspond to y_S and since $x_3(y_S)$ is identical to x_M, we obtain, from (48),

$$x_1(y_S)=\frac{2y_S}{x_M^2g(\Delta')}.$$

Similarly,

$$x_3(y_L)=\frac{2y_L}{x_m^2g(\Delta')}.$$

Thus we find the range of the bistable transmitted fields x_1 and x_3 to be

$$\Delta x_1=x_m-\frac{2y_S}{x_M^2g(\Delta')}, \tag{49}$$

$$\Delta x_3=\frac{2y_L}{x_m^2g(\Delta')}-x_M. \tag{50}$$

From Eqs. (49), (50), and (44)–(47) we can see that the bistable regions Δx_1 and Δx_3 strongly depend on the resonant factor $g(\Delta')$. From Eq. (28) we can see that $g(\Delta')$ depends not only on the frequency detuning Δ' but also on the band parameters, i.e., the dipole moments f_n and the bandwidth ξ. Thus the bistable regions Δx_1 and Δx_3 also depend not only on Δ' but also on the band parameters. Particularly, if the frequency detuning $\Delta'=0$, $g(0)=1$, the bistable regions are the same as those of the resonant two-level system. These characteristics of the bistable dye system will be clearly shown by numerical examples in the next section.

Incidentally, as shown in Ref. [5], no positive slope instability arises for $\gamma_\parallel \ll \gamma_\perp$ (i.e., the dephasing rate is much larger than the depopulation rate) in a two-level system. Similarly, from Eq. (40) we can verify that no positive slope instability exists for $\gamma_d \ll \beta$ in the band model. We infer from this point that there is no self-pulsing instability in an optical bistable dye system since $\gamma_d \ll \beta$ is always valid for typical dye molecules [6].

IV. NUMERICAL ANALYSIS

In the following numerical analysis we assume that the band is continuous and that the distribution of dipole moments f_σ, as a function of σ, is a Lorentzian function of width Γ, i.e.,

$$f_\sigma=\frac{\text{const}}{1+\sigma^2/\Gamma^2}, \tag{51}$$

where const is to be determined by the normalization condition $g(0)=1$. Equation (28) then becomes

$$g(\sigma)=\int_{-\xi}^{\xi}\frac{\text{const}}{[1+(\sigma-\Delta')^2](1+\sigma^2/\Gamma^2)}d\sigma. \tag{52}$$

In this equation, $g(\sigma)$ has three parameters, the frequency detuning Δ', the band-width ξ, and the Lorentzian width Γ. Thus Δx_1 and Δx_2 are determined by Δ', ξ, and Γ when C is given. We now study the dependence of $\Delta x_1(\Delta x_3)$ on Δ', ξ, and Γ using the numerical calculations.

Setting the bistable parameter $C=104.0$, the band-width $\xi=10.0$, and the Lorentzian width $\Gamma=20.0$, we

obtain the plots of the bistable regions Δx_1 and Δx_3 versus Δ' as shown in Figs. 4(a) and 4(b), respectively. In these figures, curve 1 corresponds to the band model, whereas curve 2 is the counterpart in the two-level model. Clearly, Δx_1 and Δx_3 are slowly varying functions of Δ' within the bandwidth. That is, the bistable regions in the band model are much the same as the situation of $\Delta'=0$ (corresponding to the resonant case in the two-level model).

With the same C ($=104.0$) as in Fig. 4, Figs. 5(a) and 5(b) represent, respectively, the bistable regions Δx_1 and Δx_3 as functions of the Lorentzian width Γ for given bandwidth ξ and frequency detuning Δ'. Figures 6(a) and 6(b) represent, respectively, the bistable regions Δx_1 and Δx_3 as functions of ξ for given Γ and Δ'. In Figs. 5 and 6, curve 1 corresponds to the frequency detuning $\Delta'=5.0$, curve 2 to $\Delta'=2.0$, and the dashed line to $\Delta'=0.0$.

We can clearly see from Figs. 5(a) and 5(b) that the bistable regions Δx_1 and Δx_3 are strongly dependent on the band parameter Γ when Γ becomes smaller, whereas Δx_1 (Δx_3) is an insensitive function of Γ and approaches the $\Delta'=0$ limit (dashed line) when Γ becomes larger. These characteristics of the relation between the bistable regions and Γ in the band model can be explained as follows. For small Γ, the distribution of the dipole moments will become sharper, so that the main contribution in the optical bistable action comes from only those few

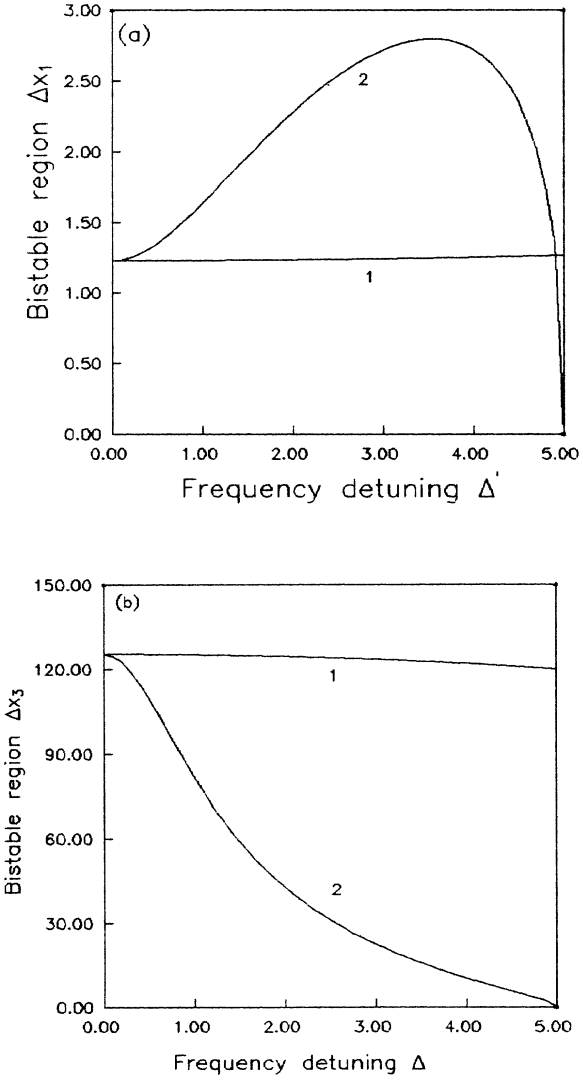

FIG. 4. Plot of the bistable region [(a) for Δx_1, (b) for Δx_3] vs the frequency detuning Δ' for $C=104.0$. Curve 1 represents the band model with bandwidth $\xi=10.0$ and Lorentzian width $\Gamma=20.0$, and curve 2 the two-level model.

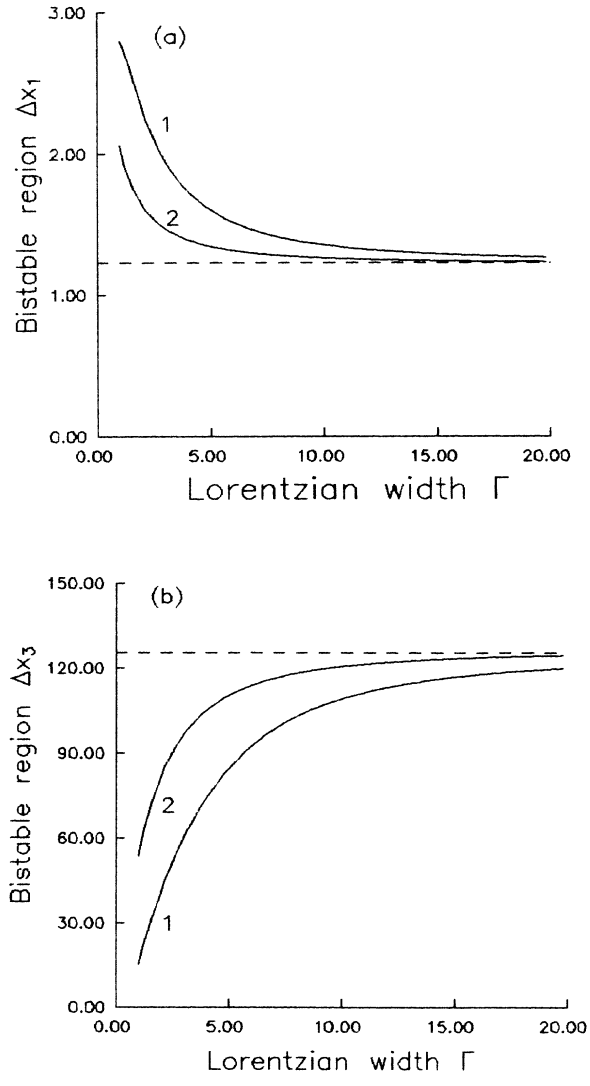

FIG. 5. Plot of the bistable region [(a) for Δx_1, (b) for Δx_3] vs Γ for $\xi=10.0$ and $C=104.0$. Curve 1 corresponds to the frequency detuning $\Delta'=5.0$, curve 2 to $\Delta'=2.0$, and the dashed line to $\Delta'=0.0$.

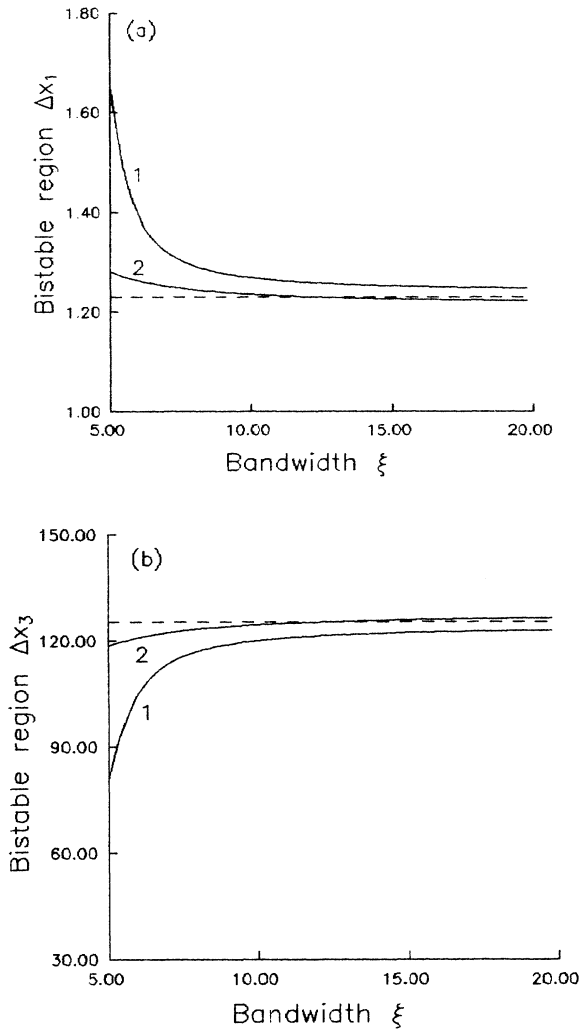

FIG. 6. Plot of the bistable region [(a) for Δx_1, (b) for Δx_3] vs ξ for $\Gamma=20.0$ and $C=104.0$. Curve 1 corresponds to the frequency detuning $\Delta'=5.0$, curve 2 to $\Delta'=2.0$, and the dashed line to $\Delta'=0.0$.

sublevels near the center of the band, and the number of the nearly resonant sublevels strongly depends on Γ. On the contrary, when Γ becomes larger, the distribution of the dipole moments will become flatter and almost all sublevels in the band structure will become relatively more active, i.e., it is easier for resonant optical transitions to the excited singlet state to occur when the detuning $|\Delta'|$ is less than the bandwidth ξ ($|\Delta'|<\xi$), thus the bistable regions tend to the situation of $\Delta'=0$, as may be seen from Fig. 5.

The plots of Δx_1 and Δx_3 in Fig. 6 are similar in behavior to the corresponding plots in Fig. 5. We may interpret them as follows: For a given detuning $\Delta(=\beta\Delta')=\omega_0-\omega$, or equivalently, a given field frequency $\omega=\omega_0-\Delta$, the contribution to the optical bistable action mainly comes from the sublevels n with transition frequencies ω_n near ω. For example, for $|\Delta'|\approx\xi$ and $\Delta'>0$ ($\Delta'<0$), the contribution comes mainly from the upper (lower) edge of the band, whereas the lower (upper) half band is in an off-resonant condition and hence its contribution is negligible. In these situations, the bistable regions Δx_1 and Δx_3 are strongly dependent on ξ. On the contrary, when ξ becomes larger, the number of active sublevels increases, the dependence is more insensitive, and finally, when $\xi\gg|\Delta'|$, the bistable regions Δx_1 and Δx_3 tend to the situation of $\Delta'=0$, as shown in Fig. 6.

V. SUMMARY

In this paper we have derived different Maxwell-Bloch equations describing the optical bistability of a dye ring cavity by taking into account the propagation effects. These equations provide a most suitable tool to study the dynamical behavior for this system. By using the linear stability analysis and numerical calculations, we have shown that the bistable regions Δx_1 and Δx_3 in the band model are slowly varying functions of the frequency detuning Δ and that the bistable regions Δx_1 and Δx_3 strongly depend on the bandwidth ξ (or the Lorentzian width Γ of the dipole-moment distribution) when ξ (or Γ) is small, whereas Δx_1 and Δx_3 are insensitive functions of ξ (or Γ) when ξ (or Γ) is large. We have thus obtained more quantitative relations for optical bistable behavior of a dye ring cavity. Moreover, we infer that self-pulsing instabilities would not be observed in bistable systems with typical dye molecules. These results are helpful for experimental studies of dye-laser systems.

ACKNOWLEDGMENTS

This work was supported by the Natural Science Foundation of China and partially supported by Grant No. LWTZ-1298 of the Chinese Academy of Sciences.

*Address for correspondence.

[1] Hong Fu and H. Haken, Phys. Rev. A **36**, 4802 (1987).
[2] L. W. Hillman, J. Krasinki, R. W. Boyd, and C. R. Stroud, Jr., Phys. Rev. Lett. **52**, 1605 (1984).
[3] Shang-qing Gong, Shao-hua Pan, and Guo-zhen Yang, Phys. Rev. A **45**, 6655 (1992).
[4] R. Bonifacio and L. A. Lugiato, Lett. Nuovo Cimento **21**, 510 (1978).
[5] L. A. Lugiato, in *Progress in Optics*, edited by E. Wolf (North-Holland, New York, 1984), Vol. XXI.
[6] Hong Fu and H. Haken, Phys. Rev. A **42**, 4151 (1990).